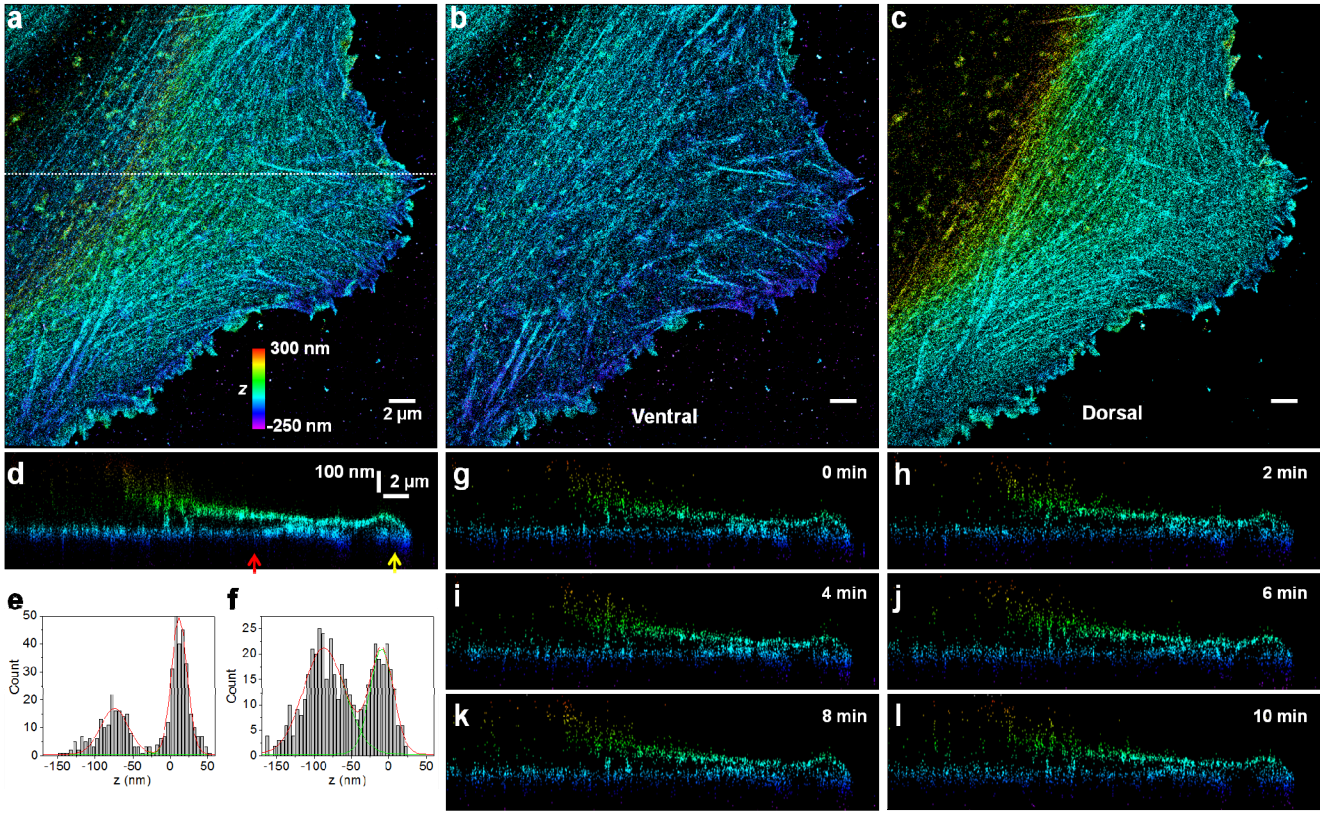

Supplementary Figure 1. Dual-objective STORM images of the actin cytoskeleton in a live BSC-1 cell. To obtain STORM images of actin in living cells, Alexa 647-labeled actin monomers were microinjected into cells and allowed to be incorporated into the cytoskeleton. The imaging buffer was D-MEM (high glucose, 25 mM HEPES, no phenol red; Invitrogen 21063) supplemented with 0.3% β-mercaptoethanol, 2% glucose, 0.8 mg/mL glucose oxidase, and 40 μg/mL catalase. This imaging buffer maintained the viability of cells[1]. Due to the highly dynamic nature of actin filaments, as well as the fact that only a fraction of the actin monomers were incorporated into the cytoskeleton while the remaining ones diffused in the cytoplasm and constituted a strong fluorescence background, the quality of these live-cell images was not as high as those of the fixed cells. Nonetheless, the two actin layers with similar thickness and vertical separation as in fixed cells were clearly resolved. (**a**) Dual-objective STORM image. (**b,c**) The ventral (**b**) and dorsal (**c**) actin layers. (**d**) Vertical cross section (500-nm wide in *y*) of the image along the dot line in (**a**). Two vertically separated actin layers are clearly resolved. (**e,f**) The *z*-profiles taken at the points corresponding to the red (**e**) and yellow (**f**) arrows in (**d**). The *z*-profile of (**f**) was taken within 1.5 μm of the cell edge. Each histogram is fit to two Gaussians (red curves), yielding FWHMs of 43 nm and 25 nm for the ventral and dorsal layers, respectively, and a peak separation of 87 nm in (**e**), and FWHMs of 65 and 37 nm for the ventral and dorsal layers, respectively, and a peak separation of 77 nm in (**f**). (**g-l**) The vertical cross section images acquired at the indicated time points. The images in (**a-d**) were acquired in 12 minutes and those in (**g-l**) were acquired in 2 minutes. The scale bars are 2 μm in (**a-c**), 2 μm for the *x-y* direction and 100 nm for the *z* direction in (**d**). The magnification in (**g-l**) is the same as that in (**d**).

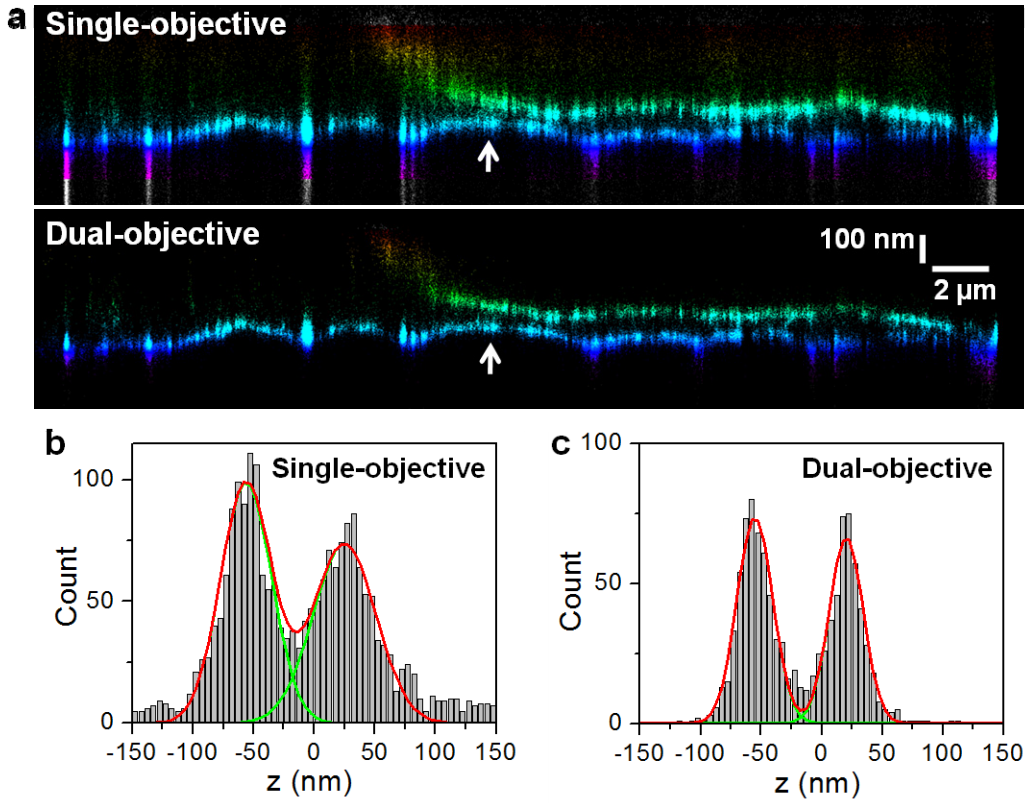

Supplementary Figure 2. Comparison between the vertical cross sections of dual-objective and single-objective STORM images obtained by the dual-objective setup. (a) Comparison of the *x*-*z* vertical cross section presented in **Fig. 3b**. (**b**,**c**) The *z*-profiles along the vertical sections, corresponding to the white arrows in (**a**). Each histogram is fit to two Gaussians (red curves), yielding FWHMs of 50 nm and 61 nm for the ventral and dorsal layers in (**b**), and FWHMs of 35 and 33 nm for the ventral and dorsal layers in (**c**). The dual-objective image shows substantially higher resolution and fewer stray localizations than the single-objective image.

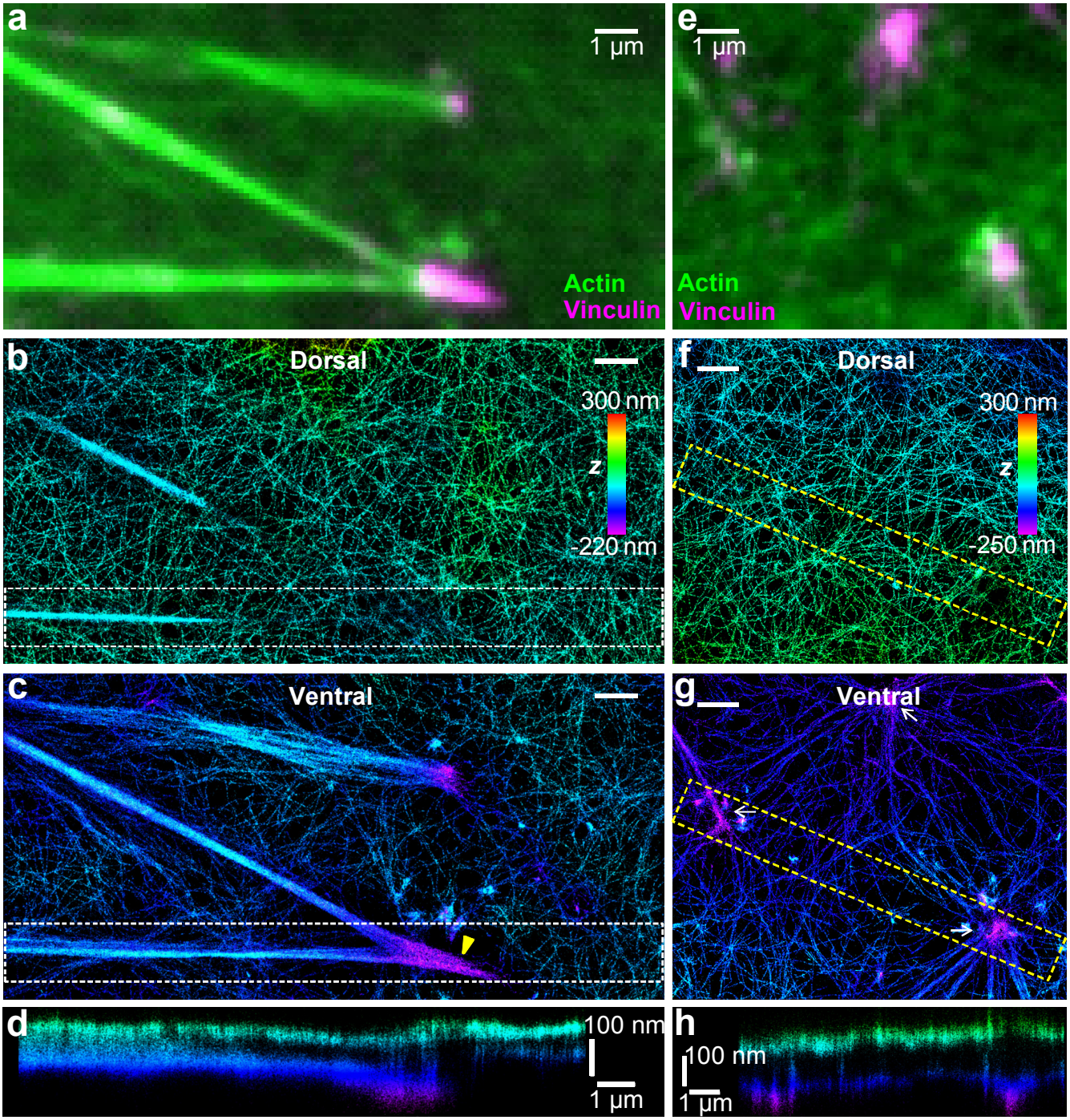

Supplementary Figure 3. Relations between the two actin layers, filament bundles, and adhesion plaques. (**a-d**) Adhesion plaques and the actin cytoskeleton in a BSC-1 cell. (**a**) Overlaid conventional fluorescent images of actin (phalloidin-labeled, green) and vinculin (immunofluorescence, magenta). Vinculin is typically used as an adhesion complex marker. (**b,c**) The dorsal and ventral actin layers revealed by dual-objective STORM. Yellow arrowhead points to an adhesion plaque that is connected to two thick linear filament bundles. (**d**) Vertical cross section along a linear bundle, corresponding to the white boxes in (**b,c**). (**e-h**) The isotropic adhesion structures (white arrows in **g**) and the actin cytoskeleton in another BSC-1 cell. (**e**) Overlaid conventional fluorescent images of actin and vinculin. (**f,g**) The dorsal and ventral actin layers revealed by dual-objective STORM. (**h**) Vertical cross section through two adhesion sites, corresponding to the yellow boxes in (**f,g**). Scale bars: 1 μm in **a-c** and e-**g**; 100 nm for *z* and 1 μm for *x/y* in **d** and **h**.

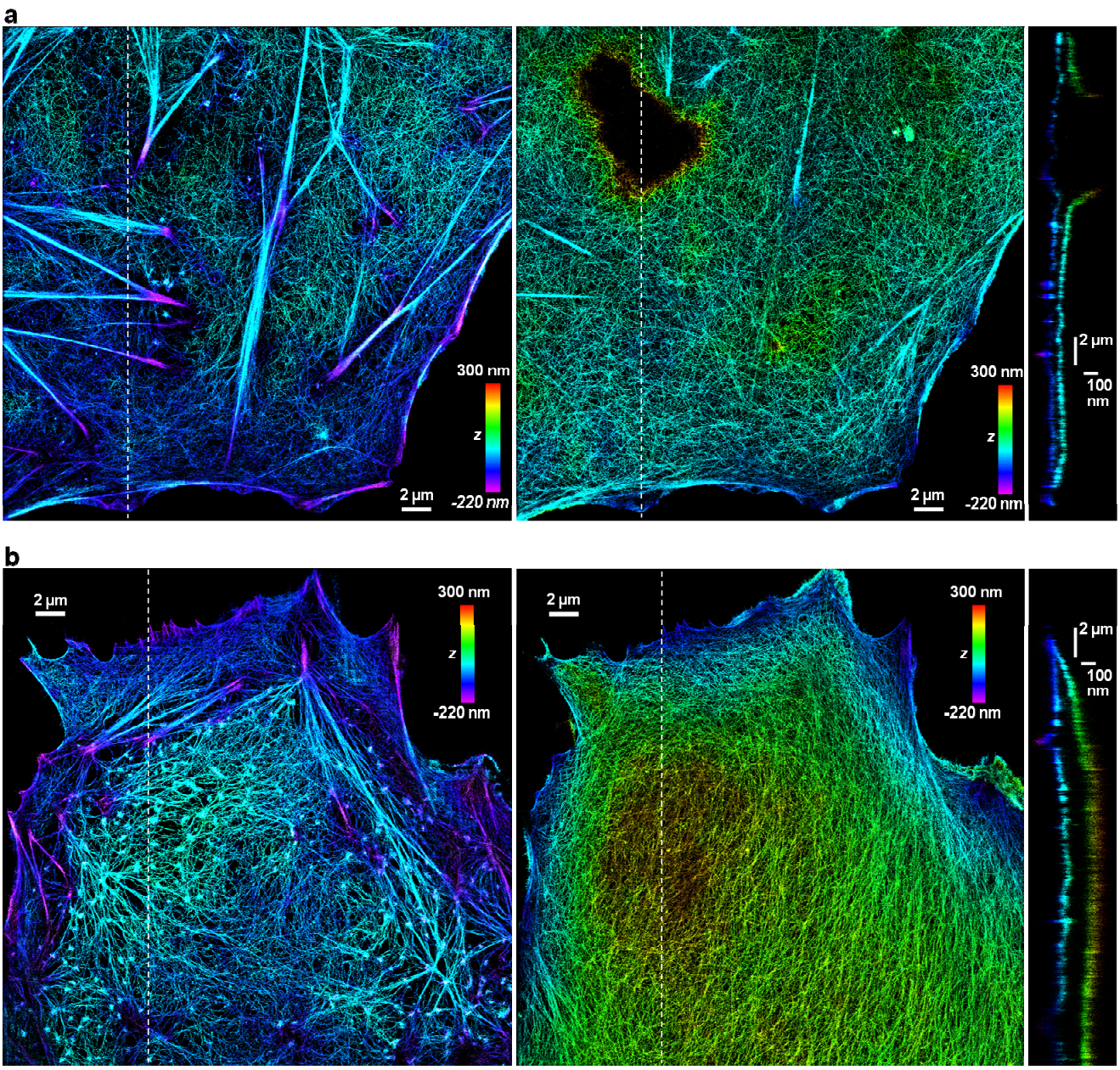

Supplementary Figure 4. Two other example images of the two-layer actin structure in the sheet-like protrusions of BSC-1 epithelial cells. (**a**) The ventral (left panel) and dorsal (middle panel) actin layers of a cell. The right panel presents the vertical cross section (500-nm wide in the *x*-*y* plane) of the cell along the lines shown in the left and middle panels. The cross section passes through a bulge-like structure, the highest part of which is out of the imaging range used in this work. (**b**) Same as (**a**) but for a different cell.

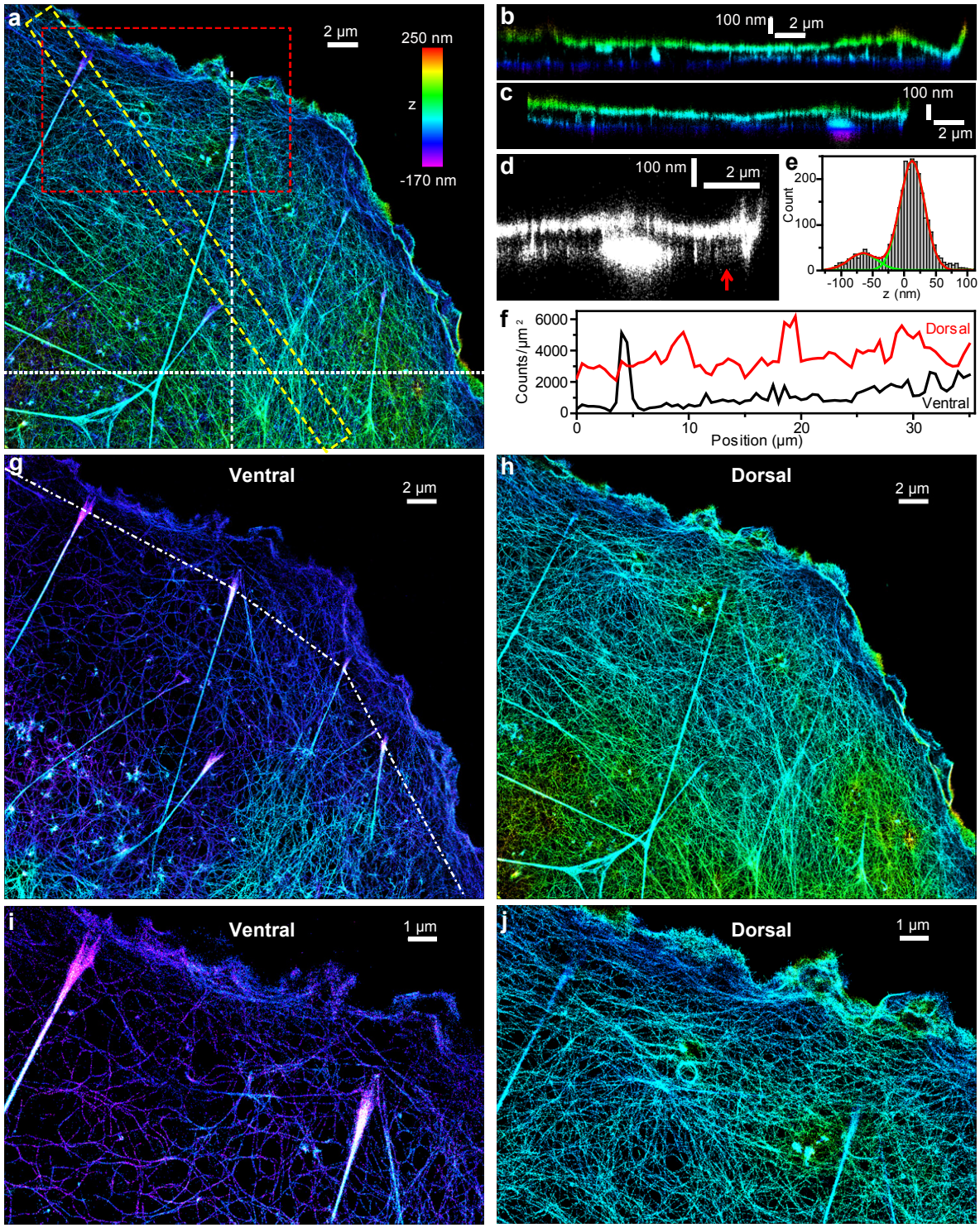

Supplementary Figure 5. The two-layer organization of actin networks in a COS-7 fibroblast cell. (**a**) Dual-objective STORM image. (**b,c**) Vertical cross sections (each 500-nm wide) along the dot and dash lines in (**a**), respectively. (**d**) Zoom-in at the cell edge for (**c**), shown in black and white with enhanced contrast. (**e**) The *z*-profile taken at the position indicated by the red arrow in (**d**). The histogram is fit to two Gaussians (green and red curves), yielding FWHMs of 53 nm and 46 nm for the ventral and dorsal layers, respectively, and a peak separation of 78 nm. (**f**) Actin density of the ventral and dorsal layers along the yellow box in (**a**), measured by the localization density. (**g,h**) The ventral and dorsal layers of actin networks. The dot-dash lines in (**g**) connects the first set of mature focal adhesions. (**i,j**) Zoom-in of the ventral and dorsal layers in the red box in (**a**).

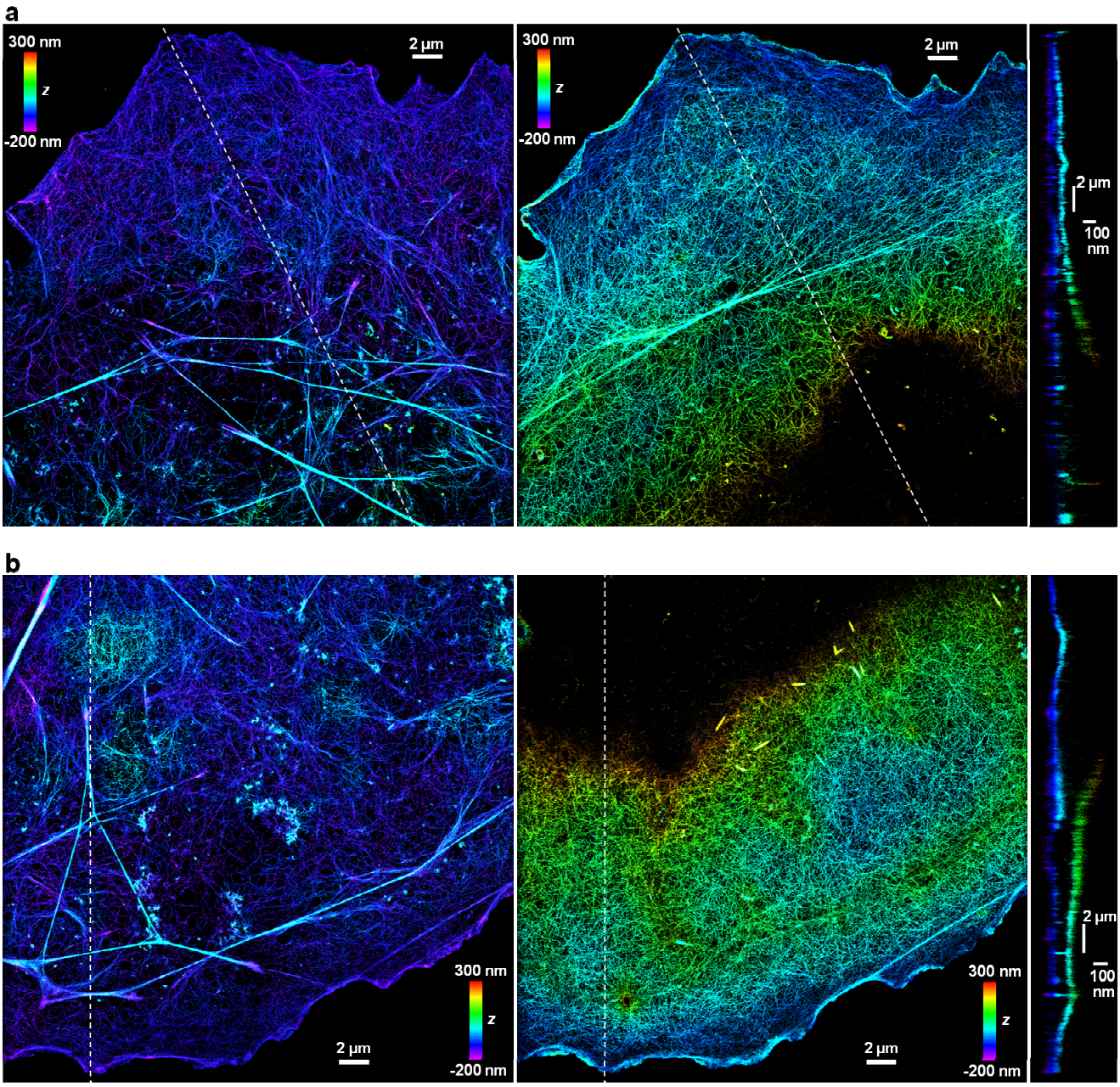

Supplementary Figure 6. Two other example images of the two-layer actin structure in the sheet-like protrusions of COS-7 fibroblast cells. (**a**) The ventral (left panel) and dorsal (middle panel) actin layers of a cell. The right panel presents the vertical cross section (500-nm wide in the *x*-*y* plane) of the cell along the lines shown in the left and middle panels. (**b**) Same as (**a**) but for a different cell. Note when far from the cell edge, the *z*-position of the dorsal layer increases quickly and falls out of the imaging range used in this work.

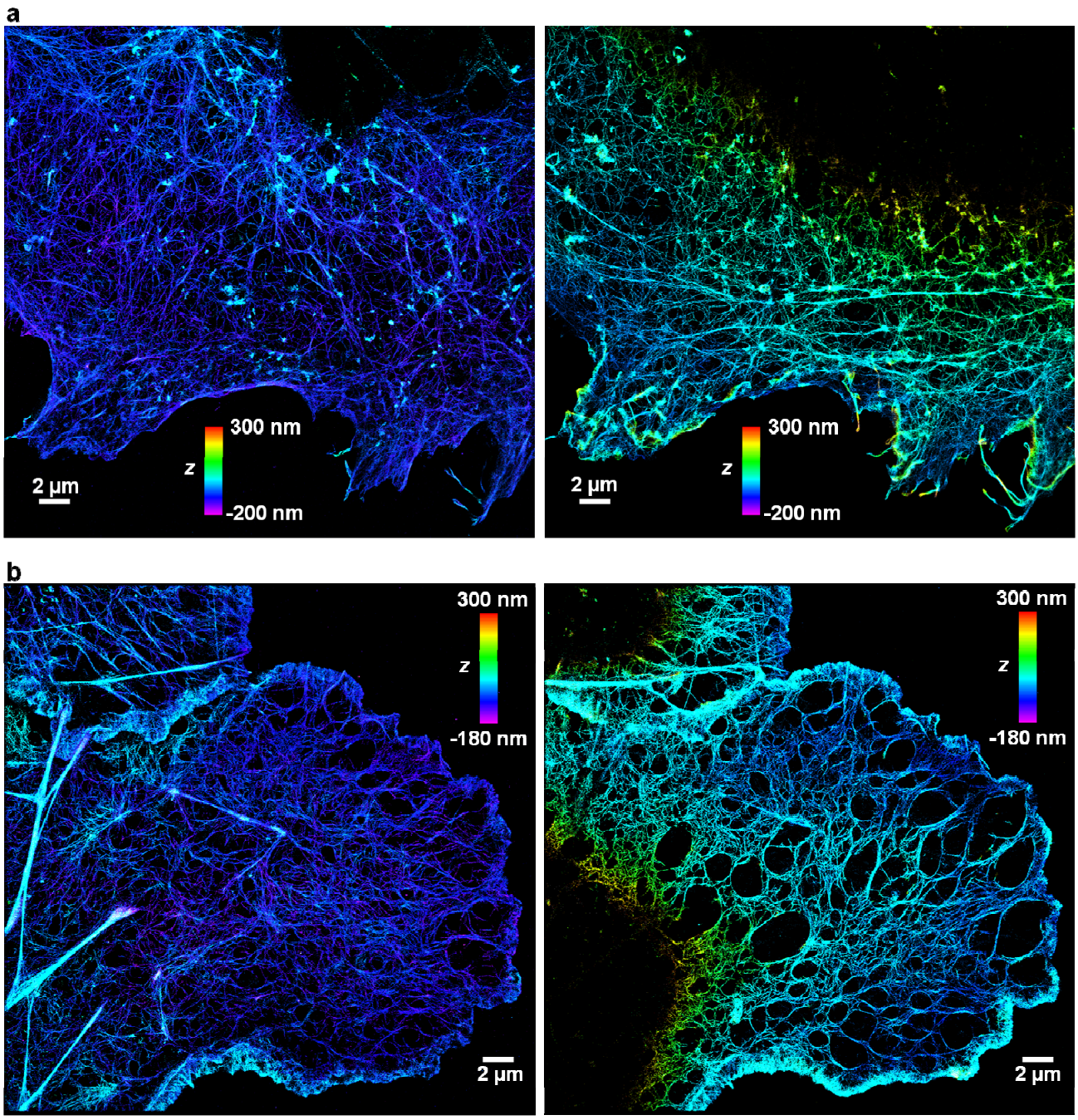

Supplementary Figure 7. Effects of cytochalasin D and latrunculin A on actin organization in the dorsal and ventral layers. (**a**) The ventral (left) and dorsal (right) actin networks of a COS-7 cell that was incubated with 0.5 µM cytochalasin D for 1 h before fixation and imaging. Cytochalastin D reduced the filament density and caused the formation of aggregates. (**b**) The ventral (left) and dorsal (right) actin networks of a COS-7 cell that was incubated with 0.25 µM latrunculin A for 1 h before fixation and imaging. Latrunculin A also reduced the filament density except for a narrow band at the extreme edge, in agreement with previous results[2]. Interestingly, the dorsal actin network was substantially more disrupted with many micron-sized voids opened up, suggesting that the dorsal layer is potentially more dynamic and thus more readily disrupted when latrunculin A depleted monomers and thereby shifted the actin dynamics towards depolymerization.

Supplementary Results. The two-layer arrangement of actin spans the lamellum and possibly extends into the lamellipodium

The sheet-like cell protrusion is comprised of a lamellipodium region at the leading edge and a lamellum connecting the lamellipodium to the cell interior[3]. Two criteria have been previously used to separate the lamellipodium and lamellum regions. First, it has been suggested that nascent adhesions initiate in lamellipodia but mature in lamella, and that the first set of matured focal adhesions in the closest proximity to the cell's leading edge marks the boundary between lamellipodia and lamella[4-6]. According to this criterion, we found that the two-layer arrangement of actin filaments spans the lamellum (**Fig. 3** and **Supplementary Figs. 4-6**) and potentially extends into the lamellipodium (e.g., **Supplementary Fig. 5d,e,g-j**). In **Supplementary Fig. 4g**, the white dot-dash line connects the first set of matured focal adhesions and the two layer arrangement of actin filaments apparently extend towards the cell edge beyond these adhesion complexes. As another criterion, previous studies has also suggested that the lamellipodium spans a ~2 μm region at the cell periphery[3,4]. By examining the actin organization within 2 μm of the cell edge, we found that the two-layer arrangement potentially extended into this region (**Supplementary Fig. 5d,e** and **Supplementary Fig. 1d,f**), though the higher actin density in this area often made it difficult to resolve the lateral organization of actin filaments at the very edge of the cell (**Fig. 3** and **Supplementary Figs. 4-6**).

Supplementary Discussion. Previous understandings of the actin filament organization in the sheet-like cell protrusions and the implications of our results.

The assembly and disassembly of actin filaments in the sheet-like structure at the cell's protrusion drive cell locomotion[7-12]. Early electron microscopy (EM) studies demonstrated that the sheet-like cell protrusion is comprised of a lamellipodium region at the leading edge and a lamellum connecting the lamellipodium to the cell interior[3]. High resolution EM has revealed the detailed lateral relationship of actin filaments, which appear to organize into a network of dense filaments in the cell protrusion[2,13-15]. It is, however, challenging to obtain a precise 3D reconstruction of actin by EM due in part to the structural perturbations induced by dehydration and embedding. While cryo-electron tomography may ultimately overcome this challenge, large volume reconstruction with cryo-tomography is still challenging and a full 3D reconstruction of the actin cytoskeleton has not yet been achieved for the entire sheet-like cell protrusion, except for the several hundred nanometers near the cell edge[15]. As a result, models of how actin is vertically organized in cell protrusions have remained inconsistent. While some models assume a vertically uniform distribution of actin filaments in the entire sheet-like cell protrusion[16,17], others speculate that actin filaments may be predominantly confined to the ventral surface to facilitate adherence to the substratum[18,19]. Fluorescent speckle microscopy studies demonstrated that the lamellipodium and lamellum actin networks are partially overlapped in space but kinematically and molecularly distinct[4]. A recent EM study suggest the presence of a dense, patchy, lamellipodium network atop a sparse, continuous, lamellum network[20]. A clear picture of how actin filaments are organized in 3D in the cell protrusions is still missing.

Our experiments revealed two vertically separated and structurally distinct actin networks in the sheet-like cell protrusion. These results in part support the previous notion that the cell's leading edge is comprised of a dense, patchy actin network situated atop of a sparse, continuous actin network[20]. Additionally, our observations showed that both networks were contiguous and extending into the cell body, and that the two layers were separated vertically by ~100 nm. Moreover, our study revealed different filament organizations for the dorsal and ventral networks. The dorsal layer appeared as a consistently dense and uniform meshwork, whereas the ventral layer exhibited lower filament density and highly variable organization.

We further found that myosin II played a key role in the structural organization of the ventral actin layer and in maintaining the structural differences between the two layers. Upon inhibition of myosin II activity, both networks became uniform actin meshworks of similar density, reminiscent of the dense, uniform dorsal network observed in untreated cells. Adhesion structures were also largely absent in the sheet-like protrusion. Recent studies indicate that myosin II plays a central role in cell migration and adhesion processes[21]. Myosin II generates retrograde flow of actin in the lamellum[4], pulls the rear of the lamellipodia actin network[20], and is important in actin bundle formation[22], adhesion complex formation[5,20], and actin network disassembly[23] during cell migration. Our finding that myosin II is important in maintaining the structural differences between the two actin layers is novel and may be related to some of these previously identified functions of myosin II.

The different structures of the two networks are likely tailored for different functions. The actin filaments in the ventral layer, which is coupled to the substratum through adhesion structures, are arranged into a web-like structure with varying organization from region to region and cell to cell, potentially responsible for the different behaviors of the cell's protrusion during locomotion. The dorsal layer, on the other hand, is only occasionally linked to the substratum (and ventral layer) through linear filament bundles, and appears as a substantially denser and more uniform meshwork, which could provide consistent mechanical support for the dorsal plasma membrane. The 3D organization of actin filaments observed here may thus help dissect the different roles of actin in the leading edge of the cell.

Supplementary Protocol 1. Setting up the dual-objective 3D STORM system

Schematic of the dual-objective 3D STORM system with further details included.

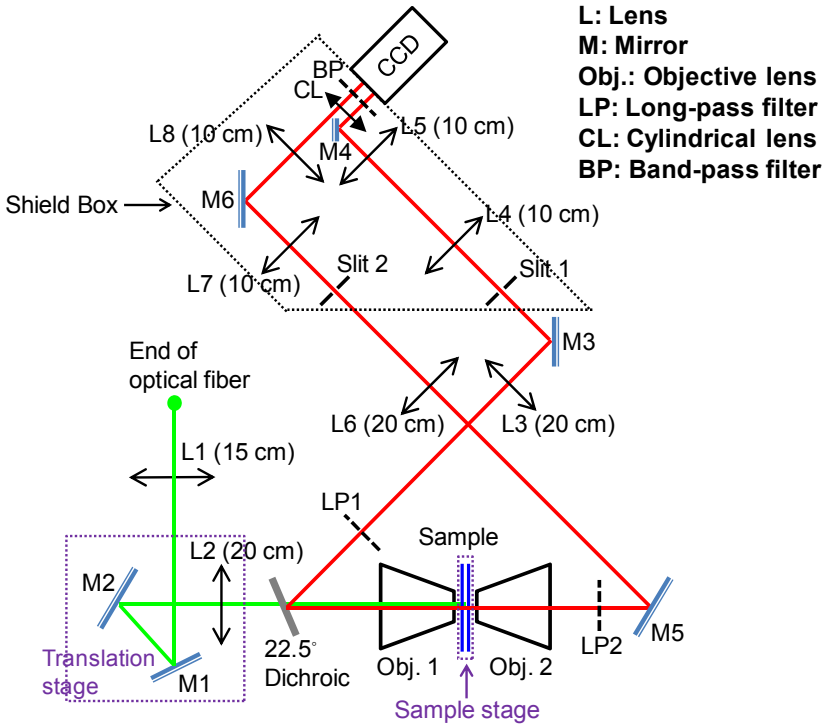

Materials required

Optical table (Newport)

Kr/Ar mixed gas laser (Innova 70C Spectrum, Coherent)

405 nm solid state laser (CUBE 405-50C, Coherent)

Dichroic mirrors and/or prisms for separating and combining lasers of different colors.

Acousto-optical tunable filter (AOTF; Crystal Technology)

Single mode fiber for 400-700 nm light (OZ Optics)

2D translation stage (for sample travel in the *xy* plane)

Two 1D translation stages (one for sample travel in *z* and one for adjusting the incident position of laser)

Piezoelectric actuator (Thorlabs DRV120)

Modular manual actuator, 8 mm differential precision adjuster (Thorlabs DRV3)

Piezo controller and strain gauge reader (e.g., Thorlabs TPZ001 and TSG00)

Z-axis translation mount (for Objective 1) (Thorlabs SM1Z)

XY translator with differential drives (for Objective 2) (Thorlabs ST1XY-D)

Two objective lenses (Olympus Super Apochromat UPLSAPO 100x, oil immersion, NA 1.40)

Customized dichroic mirror (Chroma), designed to work at an incident angle of 22.5°. This dichroic passes light for wavelengths <655 nm and reflects light for wavelengths >655 nm

Two long-pass filters (HQ665LP, Chroma)

One band-pass filter (ET700/75m, Chroma)

Two mechanical slits (Thorlabs VA100)

EMCCD camera (Andor iXon DU-897)

Cylindrical lens (Thorlabs LJ1836L1-B or LJ1144L1-B)

Achromatic lenses, with focal lengths specified in the schematic, and other routine optical components

Calibration slide (e.g., stage micrometers from Graticules)

Fluorescent beads (e.g., 1 μm crimson fluorescent beads, Invitrogen F-8816)

Computer for data collection

Procedure

1. **Laser system.** Combine different laser lines using dichroic mirrors and/or prisms (e.g., see Ref 24). For the current study using Alexa 647 dye labels, a red laser (e.g., the 647 nm line from a Kr/Ar mixed gas laser or a 656 nm solid state laser) and a violet or UV laser (e.g., a 405 nm solid state laser) are required. An AOTF may be used to control both the shuttering and the light intensity for different laser lines. Couple the combined laser lights into the optical fiber.

2. **Mounting of the sample stage.** Combine the 2D translation stage with a 1D translation stage to obtain 3D control of the sample position. For actuation of the 1D translation stage (for *z* positioning of the sample), combine a DRV120 piezoelectric actuator with a DRV3 manual actuator to obtain both a large (8 mm) working distance for coarse alignment (DRV3) and nanometer precision within a range of ~20 μm for fine adjustments (DRV120). Center the sample stage for initial alignment.

3. **Setting up the optical path (minus filters) for Objective 1.** Mount Objective 1 using a Z-axis translation mount. Use a calibration slide as the sample and illuminate from the opposite side with white light (this can be easily done as Objective 2 hasn't been installed yet at this step). Add in the 22.5° dichroic mirror and the tube lens (L3) for Objective 1, and place Slit 1 at the intermediate image formed after L3 and M3. Open the slit. Project the image onto the EMCCD camera using a pair of relay lenses (L4 and L5). Align the camera so that the center of the image is projected onto the center of the right half of the CCD. Use Slit 1 to crop the image so that when looking at the acquired camera signal on the computer screen, the image is restrained to only one half of the camera.

4. **Introduction of laser illumination.** Collimate the laser coming out of the end of the optical fiber and introduce it into the sample through the back focal plane of Objective 1. Place M1, M2, and L2 on a 1D translation stage so the laser beam can be shifted to the edge of the objective during imaging (Step 9). During initial alignment, however, pass the laser beam through the center of Objective 1 and make sure that the laser is parallel to the axis of the objective by adjusting M1 and M2. Multiple irises can be placed along the light path to check the alignment.

5. **Setting up the optical path (minus filters) for Objective 2**. Mount Objective 2 with a XY translator. Illuminate the calibration slide through Objective 1 using a weak laser and add in M5, L6, Slit 2, L7, M6, and L8 sequentially, similar to that was done for Objective 1, but project the final image onto the left half of the CCD instead.

6. **Setting up the fluorescence emission filters and cylindrical lens for astigmatism detection.** Insert the two long-pass filters (LP1 and LP2) into the two optical paths. Add in the cylindrical lens after the relay lenses (L5 and L8) of the optical paths for both Objective 1 and Objective 2. Install the band-pass filter on the camera.

7. **Alignment of fluorescent signals.** Assemble a fluorescent bead sample with coverslips on both sides. Replace the calibration slide with the bead sample. Use the 647 nm laser to illuminate the sample. Use the DRV120-DRV3 actuator system (Step 2) to adjust the *z*-position of the sample so that the beads are in focus for Objective 1. Align Objective 2 by adjusting the XY translator and the Z-axis translation mount so that Objective 1 and Objective 2 focus on the same spot of the bead sample. Make fine adjustments to Slit 1 and Slit 2 while observing the acquired camera signal on the computer screen, to ensure that the two images obtained via Objective 1 and Objective 2 each occupies one-half of the CCD without overlapping.

8. For single molecule imaging, it's essential to eliminate any background light. For this, a box can be built around the camera and the relay lenses, as illustrated in the schematic.

9. To enhance image contrast, adjust the translation stage for the incoming laser beam to shift it to the edge of Objective 1, so that the emerging light reaches the sample at incidence angles slightly smaller than the critical angle of the glass-water interface, thus illuminating only the fluorophores within a few micrometers of the coverslip surface.

10. For STORM imaging of the Alexa 647 labeled actin, use 647 nm laser (~2 kW/cm^2) to excite fluorescence from Alexa 647 molecules and switch them into the dark state. Use the 405 nm laser to reactivate the fluorophores from the dark state back to the emitting state. Adjust the power of the 405 nm laser (0-1 W/cm^2) during image acquisition so that at any given instant, only a small, optically resolvable fraction of the fluorophores in the sample were in the emitting state. See Ref 24 for more details of STORM imaging.

Supplementary Protocol 2. Cell fixation and staining for visualization of the actin cytoskeleton

Materials required

Adherent cells grown on #1.5 coverslips

Cytoskeleton buffer (CB: 10 mM MES pH 6.1, 150 mM NaCl, 5 mM EGTA, 5 mM glucose, and 5 mM $MgCl_2$)

Triton X-100

Glutaraldehyde (EM Grade; Electron Microscopy Sciences)

Sodium borohydride ($NaBH_4$)

Phosphate-buffered saline (PBS)

Alexa Fluor 647-phalloidin (Invitrogen A22287): Add 1.5 mL methanol into the vial to yield a final concentration of ~6.6 μM. This stock solution can be stored at -20 °C for a year.

Procedure

1. Culture cells on #1.5 glass coverslips. For 18-mm diameter coverslips, 12-well, flat-bottom cell culture plates (Corning costar 3513) are recommended. The liquid volumes described below are based on the size of a single well in a 12-well plate.
2. Wash the cells briefly with 1 mL of pre-warmed (37 °C) PBS.
3. Fix and permeabilize the cells using 400 μL of 0.3% glutaraldehyde and 0.25% Triton X-100 in CB for 1-2 min in the first step, followed by a second fixation step using 400 μL of 2% glutaraldehyde in CB for 10 min.
4. Treat the sample with 1 mL 0.1% $NaBH_4$ (freshly-prepared in PBS) for 7 min to reduce background fluorescence.
5. Wash with PBS for three times, each time allowing for 10-min incubation.
6. When immunofluorescence labeling of other cellular components (e.g., vinculin) is required, it is recommended that the labeling of other components is performed first and actin is labeled after the labeling of all other components is completed. Otherwise, labeled phalloidin molecules may dissociate during the extensive washing steps that are typically involved in immunofluorescence labeling.
7. To prepare the staining solution, dilute 30 μL of the Alexa 647-phalloidin stock solution into 400 μL PBS for each coverslip to be labeled. This results in a final concentration of ~0.5 μM of Alexa 647-phalloidin. Note that this diluted, aqueous staining solution should be prepared right before use. Storage of the aqueous staining solution may lead to loss of activity over days.
8. Place the staining solution on the coverslip and cover the plate lid. Wrap the plate with aluminum foil to protect from light. Incubate at 4 °C for overnight.
9. Aspirate the staining solution and briefly wash once with PBS. Immediately mount the sample for STORM imaging.

References for the Supplementary Information

1. Jones, S. A., Shim, S. H., He, J. & Zhuang, X. W. Fast, three-dimensional super-resolution imaging of live cells. *Nat. Methods* **8,** 499-505 (2011).
2. Svitkina, T. M. & Borisy, G. G. Arp2/3 complex and actin depolymerizing factor cofilin in dendritic organization and treadmilling of actin filament array in lamellipodia. *J. Cell Biol.* **145,** 1009-1026 (1999).
3. Abercrombie, M., Heaysman, J. E. M. & Pegrum, S. M. The locomotion of fibroblasts in culture IV. Electron microscopy of the leading lamella. *Exp. Cell Res.* **67,** 359-367 (1971).
4. Ponti, A., Machacek, M., Gupton, S. L., Waterman-Storer, C. M. & Danuser, G. Two distinct actin networks drive the protrusion of migrating cells. *Science* **305,** 1782-1786 (2004).
5. Choi, C. K. *et al.* Actin and alpha-actinin orchestrate the assembly and maturation of nascent adhesions in a myosin II motor-independent manner. *Nat. Cell Biol.* **10,** 1039-1050 (2008).
6. Geiger, B., Spatz, J. P. & Bershadsky, A. D. Environmental sensing through focal adhesions. *Nat. Rev. Mol. Cell Biol.* **10,** 21-33 (2009).
7. Pollard, T. D. & Borisy, G. G. Cellular motility driven by assembly and disassembly of actin filaments. *Cell* **112,** 453-465 (2003).
8. Mogilner, A. & Oster, G. Polymer motors: Pushing out the front and pulling up the back. *Curr. Biol.* **13,** R721-R733 (2003).
9. Rafelski, S. M. & Theriot, J. A. Crawling toward a unified model of cell motility: Spatial and temporal regulation of actin dynamics. *Annu. Rev. Biochem.* **73,** 209-239 (2004).
10. Small, J. V. & Resch, G. P. The comings and goings of actin: coupling protrusion and retraction in cell motility. *Curr. Opin. Cell Biol.* **17,** 517-523 (2005).
11. Chhabra, E. S. & Higgs, H. N. The many faces of actin: Matching assembly factors with cellular structures. *Nat. Cell Biol.* **9,** 1110-1121 (2007).
12. Pollard, T. D. & Cooper, J. A. Actin, a central player in cell shape and movement. *Science* **326,** 1208-1212 (2009).
13. Pollard, T. D., Blanchoin, L. & Mullins, R. D. Molecular mechanisms controlling actin filament dynamics in nonmuscle cells. *Annu. Rev. Biophys. Biomolec. Struct.* **29,** 545-576 (2000).
14. Small, J. V. *et al.* Unravelling the structure of the lamellipodium. *J. Microsc.-Oxf.* **231,** 479-485 (2008).
15. Urban, E., Jacob, S., Nemethova, M., Resch, G. P. & Small, J. V. Electron tomography reveals unbranched networks of actin filaments in lamellipodia. *Nat. Cell Biol.* **12,** 429-435 (2010).
16. Abraham, V. C., Krishnamurthi, V., Taylor, D. L. & Lanni, F. The actin-based nanomachine at the leading edge of migrating cells. *Biophys. J.* **77,** 1721-1732 (1999).
17. Atilgan, E., Wirtz, D. & Sun, S. X. Morphology of the lamellipodium and organization of actin filaments at the leading edge of crawling cells. *Biophys. J.* **89,** 3589-3602 (2005).
18. Mitchison, T. J. & Cramer, L. P. Actin-based cell motility and cell locomotion. *Cell* **84,** 371-379 (1996).
19. Mogilner, A. & Keren, K. The shape of motile cells. *Curr. Biol.* **19,** R762-R771 (2009).
20. Giannone, G. *et al.* Lamellipodial actin mechanically links myosin activity with adhesion-site formation. *Cell* **128,** 561-575 (2007).
21. Vicente-Manzanares, M., Ma, X. F., Adelstein, R. S. & Horwitz, A. R. Non-muscle myosin II takes centre stage in cell adhesion and migration. *Nat. Rev. Mol. Cell Biol.* **10,** 778-790 (2009).
22. Anderson, T. W., Vaughan, A. N. & Cramer, L. P. Retrograde flow and myosin II activity within the leading cell edge deliver F-actin to the lamella to seed the formation of graded polarity actomyosin II filament bundles in migrating fibroblasts. *Mol. Biol. Cell* **19,** 5006-5018 (2008).
23. Wilson, C. A. *et al.* Myosin II contributes to cell-scale actin network treadmilling through network disassembly. *Nature* **465,** 373-377 (2010).
24. Dempsey, G. T., Wang, W. & Zhuang, X. Fluorescence imaging at sub-diffraction-limit resolution with stochastic optical reconstruction microscopy, in *Handbook of Single-Molecule Biophysics*, edited by P. Hinterdorfer & A. Oijen (Springer New York, 2009), pp. 95-127.